J. Fluid Mech. (1996), vol. 321, pp. 299–313

Penetrative turbulent convection into a rotating two-layer fluid

By SIAVASH NARIMOUSA

Department of Mechanical Engineering, University of Southern California, Los Angeles, CA 90089–1453, USA

(Received 21 November 1995 and in revised form 29 March 1996)

Turbulent convection into stratified two-layer fluid systems in the presence of rotation has been investigated in a cylindrical laboratory tank. For a wide range of conditions the vertical stability of the flow depends only on the Richardson number $Ri = g'h_0/(B_0R)^{2/3}$ (here, $g' = g\delta\rho_i/\rho_0$ is the jump in the reduced gravity across the density interface, $\delta\rho_i$ is the jump in density itself, h_0 is the depth of the top layer, B_0 is the surface buoyancy flux and R is the radius of the source). We have found that for values of Ri greater than a critical value of $Ri_c \approx 11$, the convective flow did not penetrate through the density interface, regardless of the values of the convective Rossby number $Ro^* = \left(B_0/f^3h_0^2\right)^{1/2}$ of the flow (here f is the Coriolis parameter). In this case after the convective layer interacted with the density interface the mixed fluid, of intermediate density, propagated radially along the interface in the form of an intrusion. Later, if Ro^* was less than approximately 5, mesoscale vortices with mean diameter $D \approx 8(Ro^R)^{2/3}$ and maximum swirl velocity $v \approx (B_0R)^{1/3}$ were generated at the edge of this propagating front (here $Ro^R = \left(B_0/f^3R^2\right)^{1/2}$ is the Rossby number based on R). When Ri was less than 11, the convective flow eventually penetrated through the density interface and into the bottom layer. This occurred through the formation of discrete 'convective holes' beneath the source. At large values of Ro^*, and at early times, one turbulent plume penetrated into the bottom layer from each hole. Later the initial holes coalesced to create one large lesion beneath the source.

1. Introduction

Observations show that the upper Arctic Ocean is often stratified (Newton, Aagaard & Coachman 1974; Hunkins 1974). The stratification usually consists of a top mixed layer, of about 35–50 m depth, with a moderately sharp density jump at its base to a depth of about 80 m followed by a stratified layer of lower stability beneath, sometimes called the 'pycnocline', that extends to a depth of about 300 m. This stratified system rests on the top of a nearly homogeneous water column that then extends to great depths (2000–4000 m). During intense cooling and/or freezing of the surface of the Arctic Ocean, the resultant negative buoyancy flux generates a turbulent convective flow that penetrates through the top mixed layer and quickly interacts with the density interface. Thereafter, the fate of the convective layer depends on the values of both, the Richardson number, Ri, and the Rossby number, Ro^*, of the system.

The Rossby number $Ro^* = \left(B_0/f^3h_0^2\right)^{1/2}$ has been defined in Maxworthy & Narimousa (1994, referred to hereafter as MN), where it was introduced to describe the intensity of the convective process. B_0 is the surface buoyancy flux, f is the Coriolis

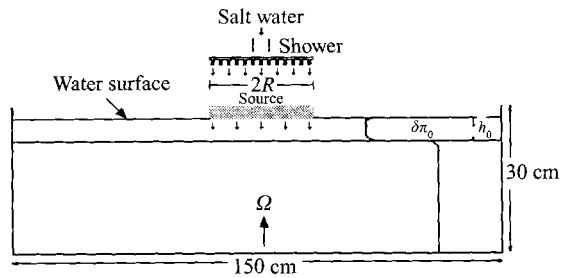

FIGURE 1. Schematic diagram of the experiment and its components.

parameter, and h_0 is the depth of the top layer. With the addition of the effect of the stratification it is necessary to introduce a Richardson number $Ri = g'h_0/(B_0R)^{2/3}$, where $g' = g\delta\rho_i/\rho_0$ is the jump in the reduced gravity across the density interface ($\delta\rho_i$ is the jump in density itself, ρ_0 is ambient density), and R is the radius of the source (see also Helfrich & Battisti 1991). Here, Ri is defined, first, in its classical form: the ratio of the buoyancy force, $g'h_0$, across the density interface to the inertia force, $(B_0R)^{2/3}$, associated with the shear flow generated as a result of the outflow from under the source. Second, and more appropriately for the interpretation of the present experiments, it is a measure of the buoyancy (or density) difference across the interface to a measure of the buoyancy or density generated by the buoyancy flux at the interface depth h_0. That is $Ri = g'/(g'_c)$, where $g'_c = (B_0R)^{2/3}/h_0$ is the buoyancy scale of the outflow from under the source given by Phillips (1966) and used extensively in MN. In order to investigate the dependency of the convective flow on both Ri and Ro^*, we have conducted many experiments for a wide range of values of them. This has enabled us to generate a graph that indicates the regions of vertical stability and instability of the system in the (Ri, Ro^*)-plane (see §4).

In the upper Arctic Ocean, mesoscale vortices with a central core of 10–20 km in diameter and velocities on the order of 30 cm s^{-1} have been detected at depths of 50–300 m (Newton *et al.* 1974; Hunkins 1974; Manley & Hunkins 1985; D'Asaro 1988). The results of the present study and those of MN enable us to present a possible explanation for the presence of these vortices (see §6). First, in §2 we describe the experimental apparatus and procedures, in §3 the experimental results, while in §4 we introduce some simple scaling arguments that are compared with the experiment in §5.

2. The experiment

The laboratory experiments were conducted in a large cylindrical tank (150 cm in diameter and 30 cm deep (figure 1). The tank was filled with two layers of salt water of slightly different densities in such a way that the top surface of the upper layer was in contact with the bottom of a circular convection source of radius $R = 12$ cm. The system was set into rotation and when it was in a solid-body rotation (counter-clockwise looking from above), the convection source, which was located at the center of the tank, was activated to release denser salt water into the less-dense top layer. Under these circumstances, the source water sank through the top layer in the form of a three-dimensional turbulent convective flow, that shortly afterwards interacted with the density interface.

In order to observe and measure the fluid motion throughout the test region both small neutrally buoyant particles (1 mm in diameter), and dye (fluorescein) were used.

To illuminate the particles and/or the dyed fluid, horizontal and vertical sheets of light were used separately. This enabled us to visualize the horizontal and the vertical structure of the convective regimes (see §3).

The quantities under our control were the depth of the upper layer (h_o); the reduced gravity across the density interface, $g' = g\delta\rho_i/\rho_0$; the rotation rate $\Omega = f/2$ s^{-1}; the density of the source fluid above ambient $\delta\rho_s$; and its flow rate Q cm^3 s^{-1}. The latter two quantities can be combined into one parameter, the buoyancy flux, $B_0 = Qg\delta\rho_s/\rho_0\pi R^2$, where ρ_0 is the density of the ambient fluid and R the radius of the source. A wide range of these four quantities (h_o, g', f and B_0) was used in order to cover as great a range of the appropriate scaling parameters, Ri and Ro^*, as possible.

3. Experimental results

3.1. *Experiments at high Ri*

As already noted, when the two-layer-system was in solid-body rotation the convection source was then activated to allow denser source water to sink into the top homogeneous layer (see §2). The three-dimensional convective layer thus formed propagated downwards until it reached the base of the mixed layer and interacted with the density interface. We found experimentally that at the high values of $Ri \gtrsim 11$ (see §4), this convective layer did not penetrate through the interface into the bottom layer but propagated radially along the base of the mixed layer in the form of a gravity current or intrusion. In this case the situation resembled the convection experiments in a homogeneous water column with a flat bottom that have been discussed comprehensively in MN. There were however some differences in detail. In the present case, the fate of the convective outflow (i.e. the gravity current) appeared to depend only on the values of Ro^*. As in MN, mesoscale vortices eventually formed at the edge of the gravity current (see figure 2). At values of $Ro^* > 3$, a single 'source' vortex always formed around the source (see figure 2*a*). Note that, in the case of convection into a homogeneous fluid and a flat, solid bottom (MN) the source vortex formed at values of $Ro^* > 1$. For values of $1 < Ro^* < 3$, two vortices always formed around the source (figure 2*b*), while the same occurred in a homogeneous fluid when $0.5 < Ro^* < 1$. At the lower values of $Ro^* < 0.5$, three or more vortices formed around the source (figures 2*c* and 2*d*). The behaviour of these mesoscale vortices was similar to that described in MN. It is believed that the difference in the values of Ro^* in the above cases arise from the fact that the effect of frictional forces on the spreading convective flow is much smaller in the present case, requiring smaller values of f (giving larger values of Ro^*) to influence the spreading convective flow.

3.2. *Experiments at moderate Ri*

At moderate values of $5 < Ri \lesssim 11$ (see §4), the convective flow did not penetrate through the density interface at first. It spread radially along the interface (figures 3*a* and 3*b*), and before generating any significant mesoscale eddies (such as those seen in figure 2) the convection flow began to penetrate into the bottom layer. Initially the penetration occurred through the formation of discrete 'convective holes' beneath the source (figure 3*c*) with a single turbulent plume emanating from each 'hole' and into the bottom layer. When they reached the bottom of the tank the individual plumes coalesced to generate a single gravity current that flowed more or less radially along the bottom (figures 3*d* and 3*e*) before becoming baroclinically unstable. The horizontal structure of these events is shown in figure 4. The first photo (figure 4*a*) shows a

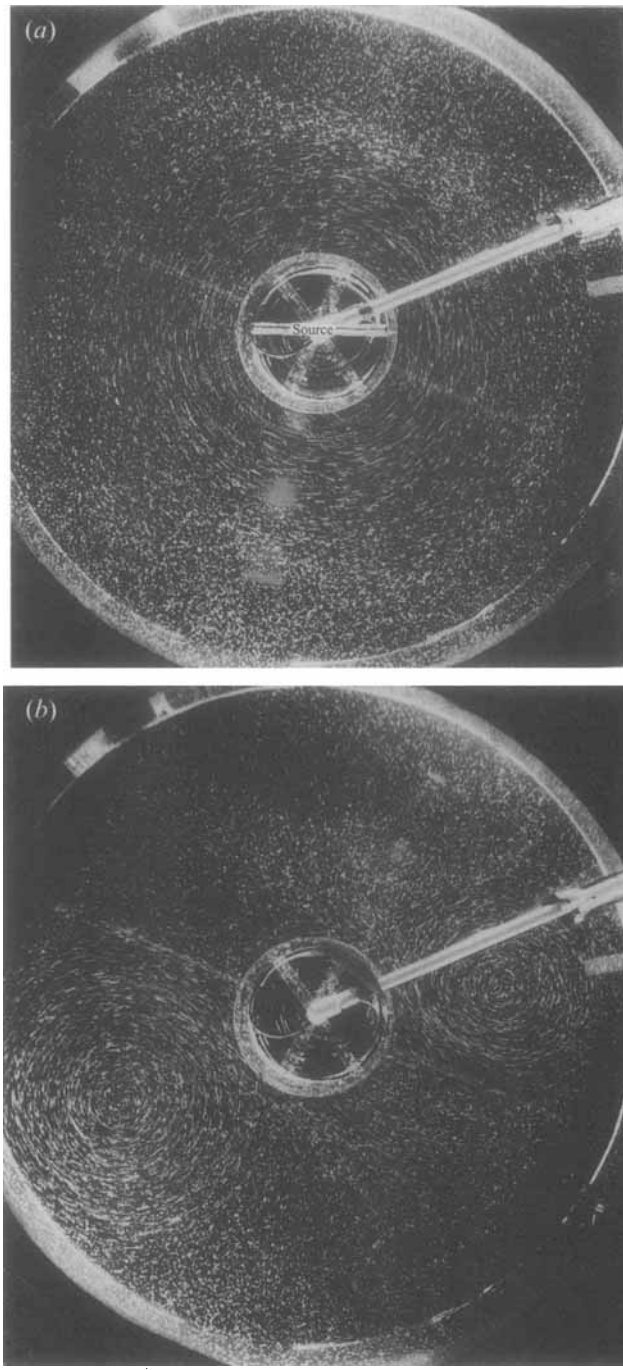

FIGURE 2. The horizontal structures of the convective vortices, for various initial conditions, that are formed around the convection source in the top layer as revealed by streak photography of neutrally buoyant particles distributed over the thickness of the interfacial layer. (*a*) A fully developed axisymmetric, cyclonic, source vortex is formed after $T = 10$ rotation period in the experiment with: $h_o = 2.5$ cm, $\delta\rho_0 = 0.037$ g cm^{-3}, $f = 0.292$ s^{-1}, $R \simeq 12$ cm and $B_0 \approx 1.73$ cm^2 s^{-3}, giving $Ro^* \approx 3.3$ and $Ri \approx 12$. (*b*) Two fully developed cyclonic vortices are formed after $T = 9$, in the experiment with: $h_o = 2.5$ cm, $\delta\rho_0 = 0.037$ g cm^{-3}, $f = 0.395$ s^{-1}, $R = 12$ cm and $B_0 \approx 1.33$ cm^2 s^{-3}, giving $Ro^* = 1.86$ and $Ri \approx 12$.

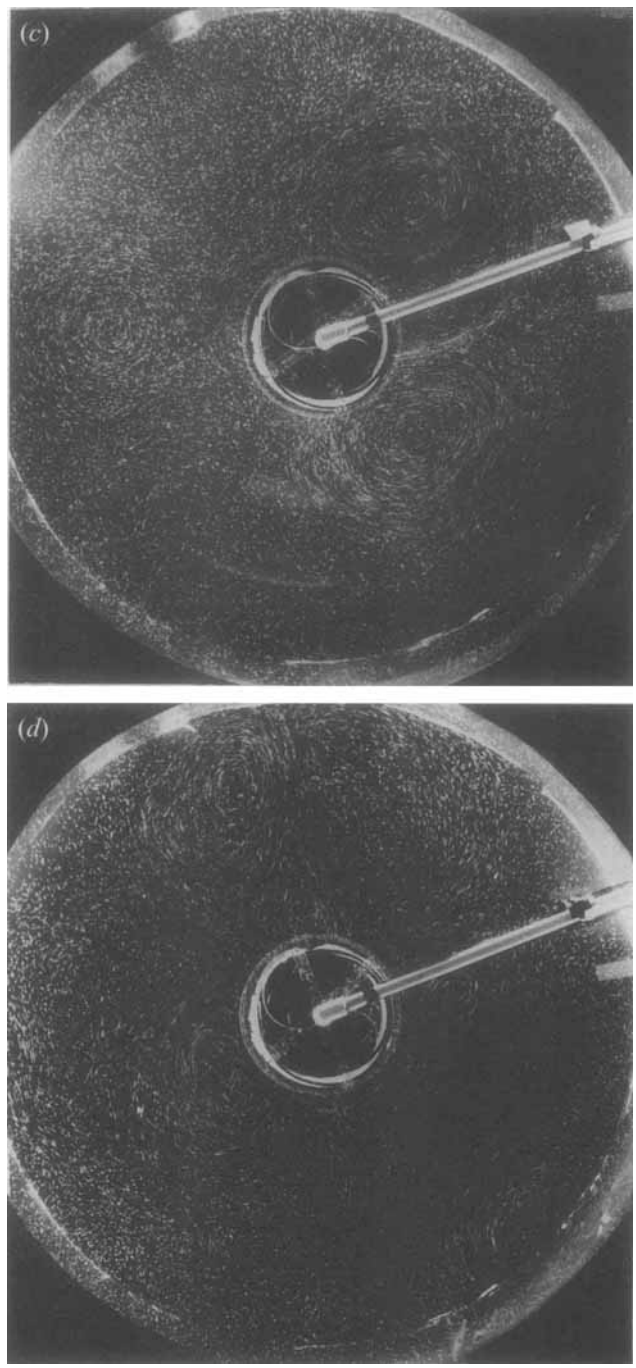

FIGURE 2. *Continued*: (*c*) Three fully developed cyclonic vortices are formed after $T = 12$, in the experiment with: $h_o = 2.5$ cm, $\delta\rho_0 = 0.037$ g cm^{-3}, $f = 1$ s^{-1}, $R = 12$ cm and $B_0 \approx 2.2$ cm^2 s^{-3}, giving $Ro^* \approx 0.78$ and $Ri \approx 17$. (*d*) Four cyclonic vortices are formed after $T = 22$, in the experiment with: $h_o = 2.5$ cm, $\delta\rho_0 = 0.037$ g cm^{-3}, $f = 1.2$ s^{-1}, $R = 12$ cm and $B_0 \approx 1.67$ cm^2 s^{-3}, giving $Ro^* \approx 0.4$ and $Ri = 12$. In these experiments $Ri \geqslant 11$, and the convective flow did not penetrate through the density interface; it propagated radially at the base of the mixed layer so that all of the vortices were generated in the top layer.

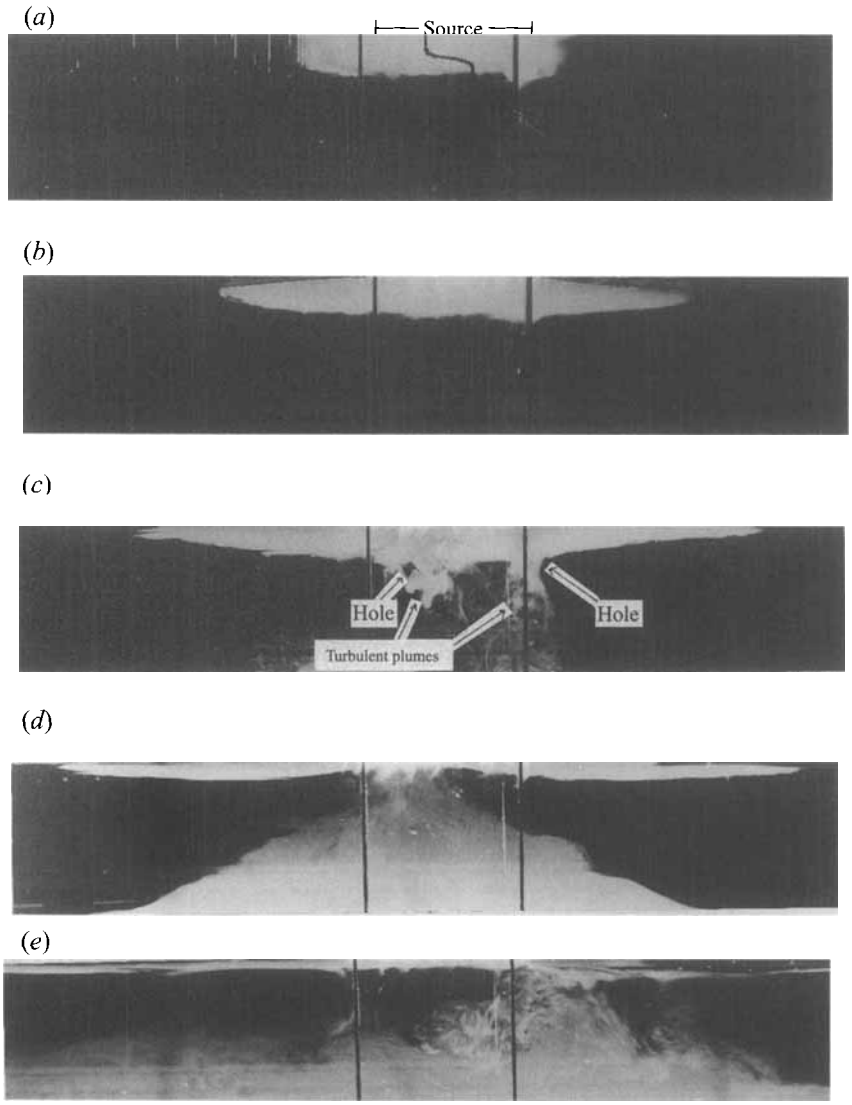

FIGURE 3. Vertical structures of the penetration of the convective flow through the density interface as revealed by dye and a vertical light source through the centre of the tank for the experiment with: $ho = 2.3$ cm, $\delta\rho_0 = 0.035$ g cm^{-3}, $f = 0.27$ s^{-1}, $R = 12$ cm and $B_0 \approx 2.92$ cm^2 s^{-3}, giving $Ro^* \approx 5.3$ and $Ri \approx 7.3$. (*a*) Taken after $T = 1/2$, showing the interaction of the convective layer with the density interface. Here, the convective layer deepens into the density interface and then spreads radially. (*b*) Taken after about $T = 1$, the convective flow continues to spread along the density interface, while no further deepening occurred beneath the source. Also, notice the inverted doming of the density interface. (*c*) Taken after about $T = 2$: two of the convective holes and the associated turbulent plumes are shown. (*d*) Taken after about $T = 4$, the convective holes have coalesced. The convective flow has interacted with the solid, flat bottom and is spreading along it (as in MN). (*e*) Taken after $T = 8$, showing the long-time behaviour of the convective flow in the bottom layer (for more detail see figure 4). Also, notice the thinning of the convective flow in the top layer as T increased, indicating that after formation of the convective hole, almost the whole convective flow has entered the bottom layer. Here, the bottom of the tank is at the bottom of the photos.

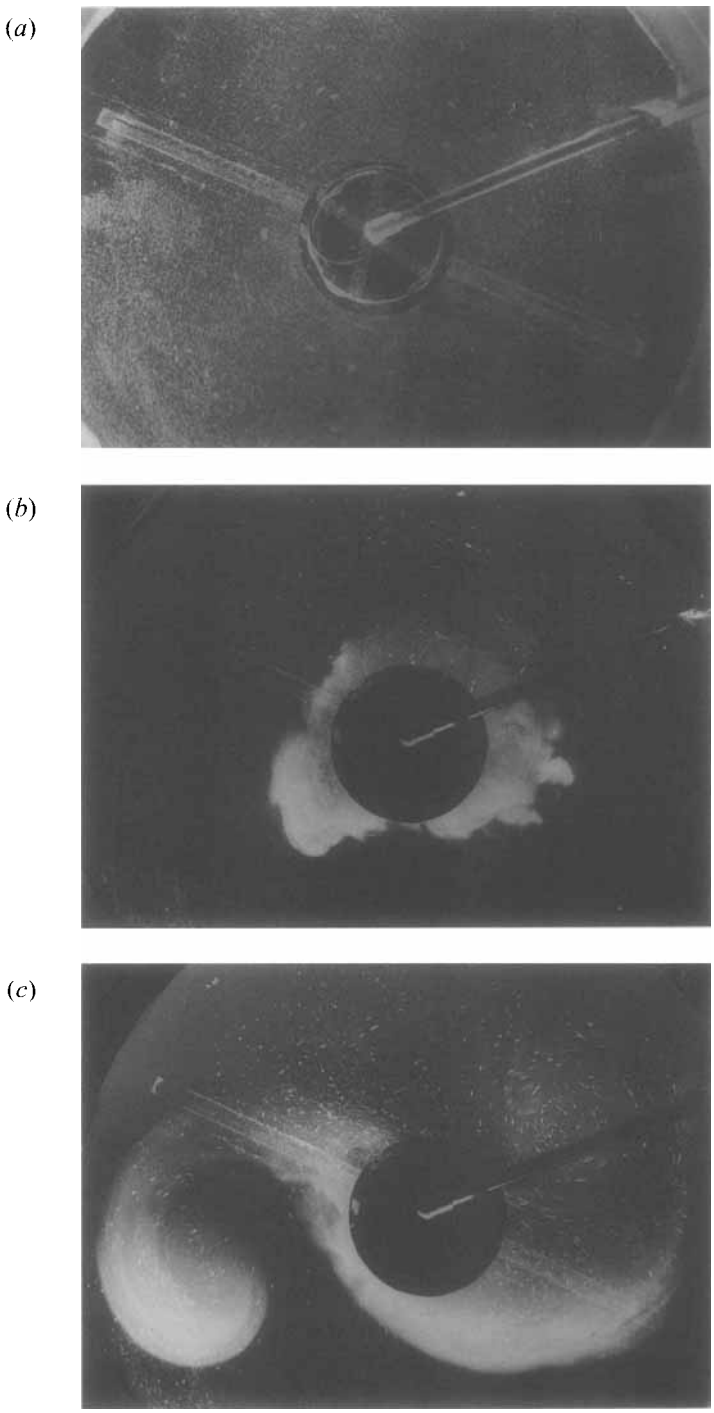

FIGURE 4. The horizontal structure of the convective events for the experiment of figure 3, as revealed by dye and streak photography of neutrally buoyant particles. (*a*) Taken after about $T = 1$ (associated with figure 3*b*), showing the formation of weak source vortex ($Ro^* \simeq 5.3$) in comparison with that shown in figure 2(*a*). (*b*) Taken after about $T = 4$ (associated with figure 3*d*), showing the spreading of the three-dimensional turbulent, convective flow along the bottom of the tank. (*c*) Taken after about $T = 8$ (associated with figure 3*e*), showing the formation of two large vortices at the bottom of the tank. It can be seen that the two vortices missed the vertical light sheet and therefore are not shown in figure 4(*e*). Only, the jet flow associated with those vortices that intersect the vertical light sheet can be seen.

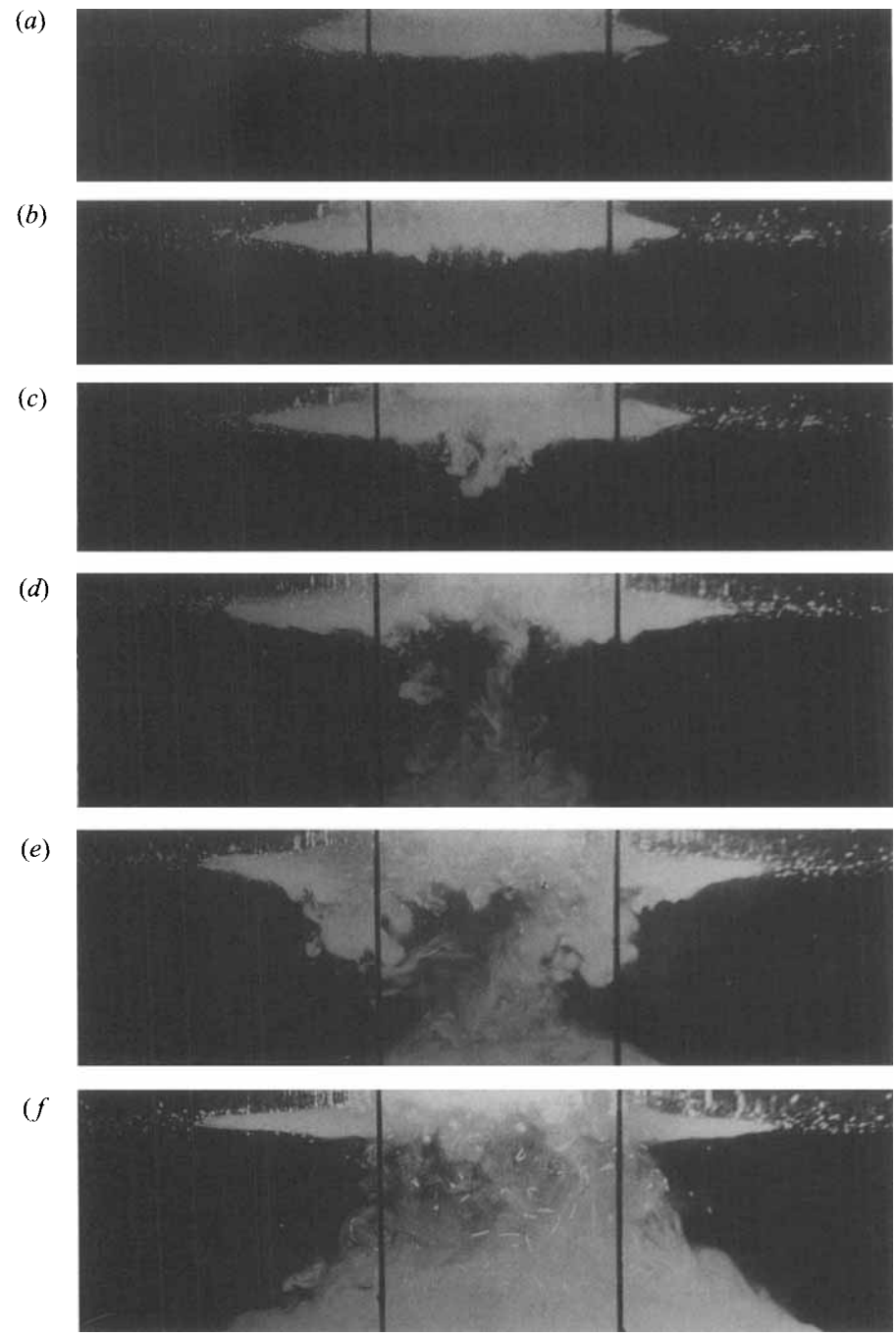

FIGURE 5. Successive photographs of the vertical structure of the convective flow through the density interface as revealed by dye and a vertical light sheet through the centre of the tank for the experiment with: $h_o \approx 2.2$ cm, $\delta\rho_0 = 0.02$ g cm^{-3}, $f = 0.287$ s^{-1}, $R \approx 12$ cm and $B_0 \simeq 2.67$ cm^2 s^{-3}, giving $Ro^* \approx 4.36$ and $Ri \approx 4.23$. (*a*) Taken after $T \simeq 0.5$, showing the horizontal spreading of the convective flow in the top layer. (*b*) Taken after $T = 1$, showing the initial penetration of the convective flow into the bottom layer. (*c*) Taken after $T = 1.25$, showing the collapse of the density interface beneath the source and turbulent penetration into the bottom layer.

weak flow field at the top of the density interface during initial spreading of the convective layer as shown in figures 3(*a*) and 3(*b*). Since this experiment has a value of $Ro^* \simeq 6$, which is larger than the critical value $Ro^* \simeq 3$, then one would expect the formation of a single, strong 'source' vortex in the top layer, similar to the one shown in figure 2(*a*). However in this case the formation of the convective holes and the associated outflow of fluid from the intrusion into the bottom layer did not permit this, so that only a weak source vortex was formed in the top layer (figure 4*a*). The second photo (figure 4*b*) shows the horizontal spreading of the convection layer on the bottom of the tank as indicated in figure 3(*d*). Eventually, when it had propagated a distance of order of the internal Rossby deformation radius the spreading front became unstable to baroclinic instabilities and two cyclonic vortices formed on the bottom of the tank (figures 4*c* and 3*e*).

At later times, the initial convection holes coalesced to create one large *lesion* beneath the source, allowing the convective flow to propagate fully into the bottom layer (figure 3*d*) and at the same time drain the initial upper-level intrusion. Under such circumstances the convective processes are similar to those in MN, and many of the findings there should apply here, too.

There were several mechanisms that contributed to the creation of the convection holes. First, and of course most critical, is that the negative buoyancy flux generated a high density at the interface. Second, the interaction of the convective flow with the density interface mixes the interface fluid upwards by turbulent entrainment. After this initial interaction the convective flow propagates radially and the resultant shear flow can further entrain the interface fluid. This reduced the density contrast across the interface so that eventually the average density of the mixed layer beneath the source reached a value comparable with that of the bottom layer. This fluid then began to penetrate through the density interface at the points where the density difference was reduced to zero and thus was able to generate the localized convective holes. In the example shown in figure 3, since the value of $Ro^* \approx 6$ was large, it took a time of less than $1/f$ for the convective holes to form.

3.3. *Experiments at low Ri*

In figure 5 we show the penetration of source fluid through the interface for a value of $Ri \approx 4.6$. In this case the initial interaction with the interface created a weak outflow the nose of which moved approximately one source radius beyond the source edge. Within one rotation period the fluid had penetrated through the interface through a single hole that rapidly grew in diameter until it covered the whole of the source area. At the same time fluid drained from the original radial outflow to reduce its thickness as seen also at the higher values of Ri for which penetration occurred (e.g. figure 3).

FIGURE 5. *Continued*: (*d*) Taken after $T = 2$, a hole as large as the size of the source has opened beneath the source and the convective flow has reached the bottom of the tank. (*e*) Taken after $T = 2.25$, the interface beneath the source has totally collapsed and the convective flow has propagated into the bottom layer. (*f*) Taken after $T = 2.75$, the convective flow has propagated along the bottom of the tank to eventually generate two cyclonic vortices similar to those shown in figure 4(*c*) and in the homogeneous case studied in MN. Here, the bottom of the tank is at the bottom of the photos.

4. Theory and scaling arguments

As mentioned in §3 when $Ri \geqslant 11$ the convective mixed layer did not penetrate through the density interface it propagated radially and eventually mesoscale vortices were generated in the top layer (figure 2). Under such circumstances, the structure of the convective flow in the top layer is similar to those observed in MN. Consequently, their scaling arguments can be used to predict the maximum swirl velocity v and the mean diameter D of the vortices generated in the present study (figure 2*a–d*). Therefore, using the Phillips (1966) criterion for density g_c' of the outflow from under the source $g_c' \sim (BoR)^{2/3}/h_0$ and the fact that the vortex diameter D scales with the local Rossby deformation radius $L_R = (g_c' h_0)^{1/2}/f$, we find

$$D/R \sim (Ro^R)^{2/3}, \tag{4.1}$$

where $Ro^R = (B_0/f^3R^2)^{1/2}$ is the Rossby number based on R.

Using the thermal wind equation ($fv = -g_c' \mathrm{d}h/\mathrm{d}r$), the swirl velocity within those vortices is

$$v \sim (B_0 R)^{1/3}. \tag{4.2}$$

For details of (4.1) and (4.2) see MN and Narimousa (1996).

For the convective flow to penetrate through the density interface and into the bottom layer, its density g_c' should be greater than or equal to the density of the bottom layer g', that is

$$g_c' \geqslant g'. \tag{4.3}$$

In Narimousa (1996), we found experimentally that

$$g_c' \approx 10(B_0R)^{2/3}/h_0. \tag{4.4}$$

Substituting for g_c' from (4.4), we obtain

$$Ri_c = \frac{g'h_0}{(B_0R)^{2/3}} \approx 10, \tag{4.5}$$

that is, when the critical Richardson number $Ri_c \approx 10$, the convective flow will penetrate into the bottom layer.

5. Experimental measurements and comparison with theory

5.1. *The Ri,Ro* graph of vertical stability*

To obtain a critical value of Ri, which separates the stable from the unstable cases in a given set of experiments with constant ho and $\delta\rho_0$, the values of B_0 and f were varied. Each case was classified as being either unstable, i.e. penetration occurred to the bottom layer, or stable in which case no penetration occurred. This process was repeated for other values of h_o and $\delta\rho_0$ and enabled us to obtain a whole range of values of Ri and Ro^* which could be classified in the same way. Then each set of values was plotted as shown in figure 6. In general one might expect that the fate of the convective flow depended on the values of both Ri and Ro^*. However, as demonstrated in figure 6, over the whole range of values of Ro^* investigated we have found that the vertical stability of the flow depended only on Ri. Thus for values of Ri greater than a critical value of $Ri_c \approx 11$, the convective layer did not penetrate through the density interface, regardless of the values of Ro^* (figure 6). When $Ri \lesssim 11$, the convective flow penetrates into the bottom layer, which is slightly larger than the condition found theoretically (i.e. 4.5). The reason for this is most likely that a

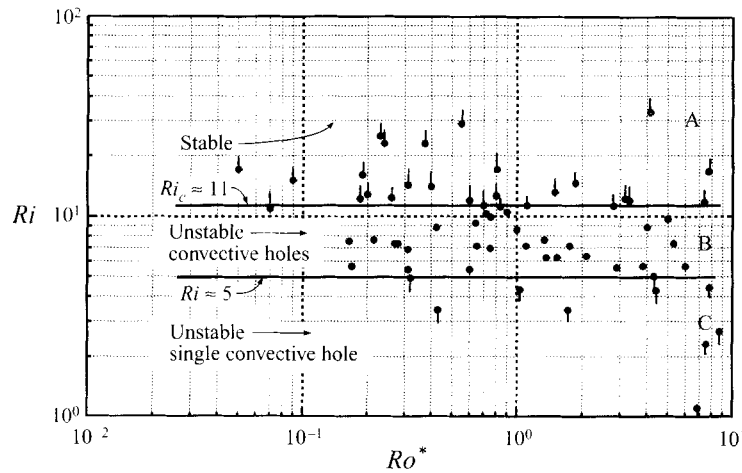

FIGURE 6. Variation of the values of Ri with associated values of Ro^*; As shown, these data have been separated into three regions A, B and C. Region A (•) is the stable region and represents the experiments in which the convective flow will not penetrate through the density interface. Region B (•) is the unstable region and represents the experiments in which the convective flow will penetrate through the density interface in the form of convective holes. Regions A and B have been separated by the straight line at $Ri \approx 11$. Region C (•) represents a very unstable flow which the convective flow penetrated through the density interface in the form of one large convective hole. The two unstable regions have been separated by the straight line at Ri ≈ 4.5.

slightly larger value of the density, produced at *ho*, was needed in order to mix with the lighter interface of fluid and generate buoyancy that could just penetrate into the bottom layer.

For the moderate values of $5 \lesssim Ri \lesssim 11$, the convective flow eventually penetrated through the density interface through the convective holes discussed in §3.2. At large Ro^* these holes were formed at early times, while at lower Ro^* the holes were formed at later times in any given experiment. At low Ro^*, initially all the convective flow propagated radially along the interface, which resulted in a situation similar to that shown in figure 2 and discussed in §3.1. After the holes were formed, some of the convective flow entered the bottom layer. At large Ro^*, the convective flow was not able to generate any significant mesoscale flow field in the top layer because almost all of the convective flow entered the bottom layer (figure 3). At the low values of $Ri \lesssim 5$ the convective plume formed a weak radial flow but then penetrated the interface within one rotation period through a single hole that quickly grew in radius.

5.2. *Vortex diameter*

We have measured the mean diameter (D) of the fully developed mesoscale vortices in the top layer for when $Ri > 11$ (figure 2). We have then plotted the values of D/R as a function of $(Ro^R)^{2/3}$ according to relationship (4.1), as shown in figure 7. The data in figure 7 support the theoretical prediction (4.1) and yield

$$\frac{D}{R} \approx 8\,(Ro^R)^{2/3} \tag{5.1}$$

which is almost the same as that found in MN when the vortices are formed on a flat, solid bottom. The solid line shown in figure 7 is the average of the data taken from Narimousa (1996) which is in agreement with the data measured for the vortices of the present case.

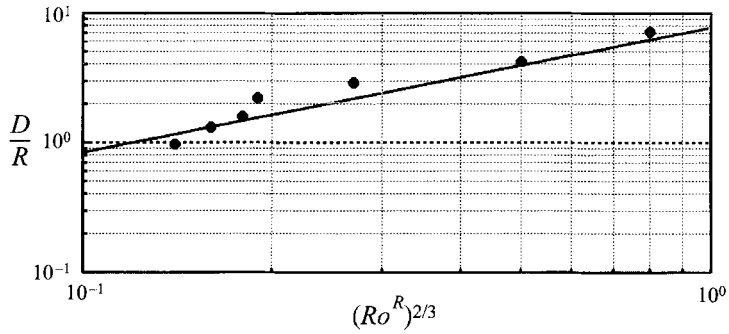

FIGURE 7. Variations of the mean diameter (D/R) of the mesoscale vortices with $(Ro^R)^{2/3}$.

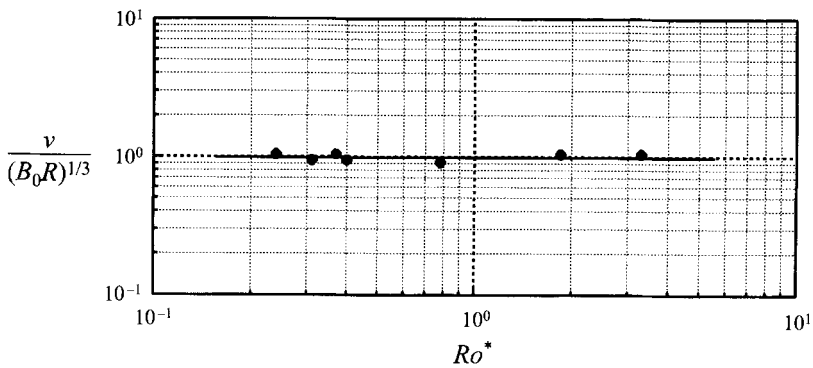

FIGURE 8. Variations of the maximum swirl velocity (v) of the mesoscale vortices normalized with $(B_0R)^{1/3}$, against Ro^*.

5.3. *Vortex velocity*

We have measured the maximum horizontal velocities within the vortices and plotted the results according to relationship (4.2), as shown in figure 8. It can be seen that the data in figure 8 support the theoretical prediction (4.2) and give

$$v \approx (B_0R)^{1/3} \tag{5.2}$$

which is the same as that found in Narimousa (1996).

6. Geophysical applications

6.1. *The Arctic Ocean*

Field measurements of density stratification (σ_t) in the upper layers of the Central Arctic Ocean revealed a typical density profile (figure 9) for this region (Newton *et al.* 1974; Hunkins 1974). If we calculate the values of Ri and Ro^*, based on the total density jump across the layer (see figure 9) with $g' = 4$ cm s^{-2}, at an average depth of about $h_0 = 125$ m, we find $Ri = 50$ and $Ro^* = 2.6$. In these calculations, we have considered a convection source with a radius of $R = 100$ km, with a typical buoyancy flux $B_0 = 3 \times 10^{-3}$ cm^2 s^{-3}, and a Coriolis parameter of $f = 1.4 \times 10^{-4}$ s^{-1}. Clearly a whole range of values could be considered but the ones given here are thought to be typical of scales found in the Arctic system. Since the value of Ri found here is

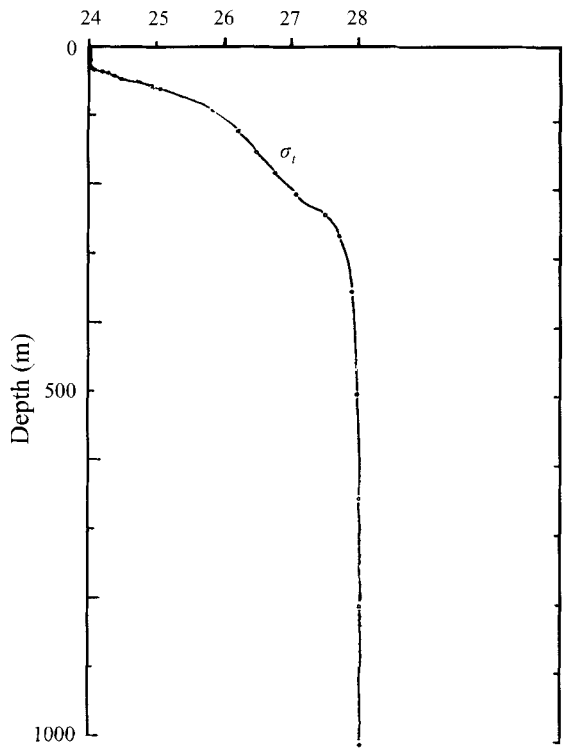

FIGURE 9. Typical vertical variations of density (σ_t) with depth in the upper layers of the open Arctic ocean (with permission from Hunkins 1974). Notice the initial steeper density variation at average depth of about 50 m, and the less stable pycnocline beneath that extends to a depth of about 300 m. This profile was taken on March, 1972 at 75°07' N 149°00' W.

greater than Ri_c, we anticipate that the convective layer will not penetrate into the deep Arctic.

Using equations (5.1) and (5.2) we estimate the mean diameter $D \approx 16$ km and the maximum swirl velocity $v \approx 30$ cm s^{-1} of the mesoscale vortices in the upper layers of the Central Arctic Ocean. These estimates are in agreement with the observed ($D = 10$–20 km and $v \approx 30$ cm s^{-1}) values (see Newton *et al.* 1974, for example).

6.2. *The Central Greenland Sea*

Schott, Visbeck & Fischer (1993) reported field measurements of deep convection in the Central Greenland Sea (away from bottom topography and coastal currents) during the winter of 1988–1989. They found that due to previous convection events a mixed layer of depth of about $ho \approx 350$ m (figure 10) over a horizontal scale of radius of about $R \approx 25$ km was formed over a weakly stratified water column beneath. Assessment of their salinity profile with depth suggest that the above stratification can be considered as a nearly two-layer-stratified system. This system then underwent cooling over a period of about 10 days (March 6–16), which resulted in downward velocities on the order of 3 cm s^{-1} at a depth of approximately 1400 m. From the above field data we estimate $Ri \approx 7.8$, and $Ro^* \approx 0.42$, based on $g' = 0.03$ cm s^{-2}, $h_o = 350$ m, $R = 25$ km, $B_0 \approx 6 \times 10^{-4}$ cm^2 s^{-3} and $f = 1.4 \times 10^{-3}$ s^{-1}. Since the value of Ri found here is smaller than Ri_c (see figure 6), the convection layer should penetrate through the interface and into the deep Central Greenland Sea. The value

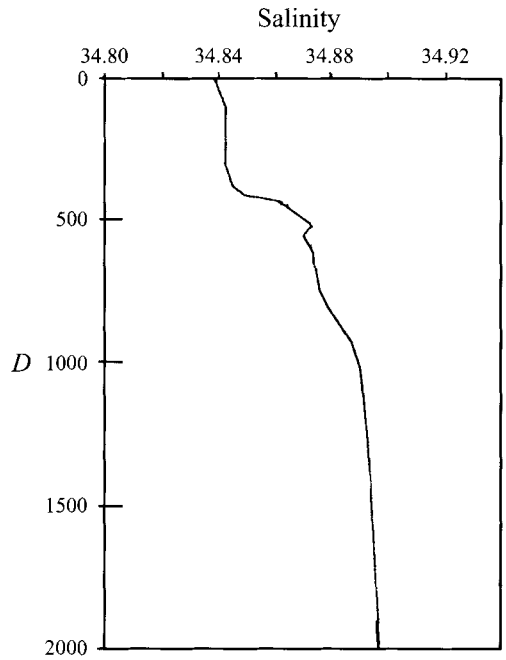

FIGURE 10. Variation of salinity with depth from the Central Greenland Sea on February 8, before the onset of a convective event (from GSP Group, 1990, as depicted in Schott *et al.* 1993).

of $Ro^* \approx 0.42$, suggests that the three-dimensional turbulent convective flow should propagate to a depth of about $z_c \approx 2$ km, before it is affected by rotation (see MN). Narimousa (1996), among others, has found that the vertical velocity (u) is given by $u \approx (0.6 \pm 0.1)(B_0 h)^{1/3}$, which gives a range of values of u from 2.2 to 3 cm s^{-1} at a depth of 1400 m. This model prediction is consistent with field observations quoted above.

7. Summary and conclusions

Deep turbulent convection in stratified two-layer-fluid systems has been investigated in a laboratory tank. A critical value of the Richardson number $Ri_c \approx 11$, has been found: that is for values of $Ri \gtrsim 11$, the convective layer did not penetrate through the density interface and into the bottom layer, regardless of the values of the Rossby number, Ro^*, of the system (see §5, figure 6). Under such circumstances, the convective layer after interacting with the density interface spread radially along the density interface in the form of a gravity front. This front then underwent a baroclinic instability and depending on the value of Ro^*, a single source vortex or several mesoscale vortices could be formed around the source (see figure 2). These mesoscale features were similar to those observed in MN. In the present study, a source vortex was generated at values of $Ro^* > 3$, while in the homogeneous case of MN the same occurred at $Ro^* > 1$.

When $Ri \lesssim 11$, the convective layer eventually penetrated through the density interface and into the bottom layer. The invasion of the bottom layer by the convective flow was accomplished through discrete convective holes that were created beneath the source (see §3.2). At large values of Ro^*, one turbulent plume penetrated into the bottom layer from each hole (see figure 3). Later in the experiment, the holes

coalesced to create one large lesion beneath the source. As the value of Ri decreased from the value of 12 the initial number of holes decreases until at around $Ri \sim 5$ only one was formed. At the same time the extent of the outflow at the top of the density jump decreased. Based on available evidence, e.g. Chu & Gascard (1991), we might tentatively identify the convective holes and the associated flow found in these experiments with the convective chimneys discussed in the literature.

Application of these modelling results to convection events in the upper layers of the open Arctic Ocean and the Central Greenland Sea has produced encouraging results. We have estimated the values of $Ri = 50$ and $Ro^* \approx 2.6$ for the upper Arctic, based on the total density jump across the layer (see §6.1, figure 9). Since $Ri = 50 > 12$ then according to our model the convective layer should not penetrate into the deep Arctic beyond 300 m. Also, we have estimated the value of the diameter $D \approx 16$ km and horizontal velocity $v \approx 30$ cm s^{-1} for the vortices of the Arctic Ocean. All of these predictions are consistent with the field observations and measurements of the vortices in the upper layers of the Arctic, as reported by Newton *et al.* (1974) and Hunkins (1974), for example.

Finally we have estimated the values of $Ri = 7.8$ and $Ro^* = 0.42$ for the Central Greenland Sea, based on the initial density jump at a depth of about 350 m (see §5.2, figure 10). In this case the turbulent convective layer should penetrate through the density interface and into the deep Greenland Sea. We estimate that the value of the vertical, downward velocity is in the range $2.2 \leqslant u \leqslant 3$ cm s^{-1} at depth 1400 m, which is consistent with the $u = 3$ cm s^{-1} reported by Schott *et al.* (1993).

We gratefully acknowledge the support of the Office of Naval Research (Grant N00014-93-1-0489) and the National Science Foundation (Grant OPP-920-7822).

REFERENCES

Chu, P. C. & Gascard, J. C. 1991 *Deep Convection and Deep Water Formation in the Oceans.* Elsevier.

D'Asaro, E. A. 1988 Generation of sub-mesoscale vortices: A new mechanism. *J. Geophys. Res.* **93**, 6635–6693.

GSP Group, Greenland Sea Project 1990 A venture toward improved understanding of the ocean's role in climate. *EOS Trans. AGU* **71**(24), 750–755.

Helfrich, K. R. & Battisti, T. M. 1991 Experiments on baroclinic vortex shedding from hydrothermal plumes. *J. Geophys. Res.* **96**, 12511–12518.

Hunkins, K. L. 1974 Subsurface eddies in the Arctic Ocean. *Deep-Sea Res.* **21**, 1017–1033.

Manley, T. O. & Hunkins, K. L. 1985 Mesoscale eddies of the Arctic Ocean. *J. Geophys. Res.* **70**, 4911–4930.

Maxworthy, T. & Narimousa, S. 1994 Unsteady, turbulent convection into a homogeneous rotating fluid, with oceanographic applications. *J. Phys. Oceanogr.* **24**, 865–887 (referred to herein as MN).

Narimousa, S. 1996 The stability and dynamics of meso-scale vortices generated by turbulent convection at large aspect ratios. submitted.

Newton, J. L., Aagaard, K. & Coachman, L. K. 1974 Baroclinic eddies in the Arctic Ocean. *Deep-Sea Res.* **31**, 707–719.

Phillips, O. M. 1966 On turbulent convection currents and the circulation of the Red Sea. *Deep-Sea Res.* **13**, 1149–1160.

Schott, F., Visbeck, M. & Fischer, J. 1993 Observations of vertical currents and convection in the Central Greenland Sea during the winter 1988–1989. *J. Geophys. Res.* **98**, 14401–14421.